Measuring the Size Dependence of Young's Modulus Using Force Modulation Atomic Force Microscopy†

William J. Price,‡ Shannon A. Leigh,‡ Stephen M. Hsu,§ Timothy E. Patten,‡ and Gang-yu Liu*,‡

Department of Chemistry, University of California, Davis, California 95616, and National Institute of Standards and Technology, Gaithersburg, Maryland 20899-8520

Received: August 9, 2005; In Final Form: October 17, 2005

The dependence of the local Young's modulus of organic thin films on the size of the domains at the nanometer scale is systematically investigated. Using atomic force microscopy (AFM) based imaging and lithography, nanostructures with designed size, shape, and functionality are preengineered, e.g., nanostructures of octadecanethiols inlaid in decanethiol self-assembled monolayers (SAMs). These nanostructures are characterized using AFM, followed by force modulation spectroscopy and microscopy measurements. Young's modulus is then extracted from these measurements using a continuum mechanics model. The apparent Young's modulus is found to decrease nonlinearly with the decreasing size of these nanostructures. This systematic study presents conclusive evidence of the size dependence of elasticity in the nanoregime. The approach utilized may be applied to study the size-dependent behavior of various materials and other mechanical properties.

Introduction

The development of the next generation of devices, chips, and micro- and nanoelectromechanical systems (MEMS and NEMS) demands advances in nanoscience and nanoengineering.[1−3] Determination of the mechanical properties of nanostructures has received increasing attention lately due to the rapid development of nanotechnology and the successful fabrication of many nanodevices and components.[4−7] Measurement of local hardness, elasticity, and shear modulus of materials at the nanometer scale, however, is fraught with both theoretical and experimental challenges. Many of the current models of mechanical properties are based on continuum mechanics models.[8−10] As the size scale shrinks toward atomic and molecular dimensions, questions arise if quantum mechanics models are necessary to predict and explain the responses of the atomic and molecular clusters and assemblies.[11,12]

It is relatively well-known that materials exhibit size-dependent optical, electronic, and magnetic properties when the features approach nanometer dimensions, such as quantum dots or nanoparticles.[13−20] Understanding these size-dependent observations often requires quantum mechanics theory.[21,22] It has long been conjectured that analogous size-dependent mechanical properties may exist when the local structures approach smaller and smaller sizes as suggested by molecular dynamics and quantum models.[23−25] Unlike size-dependent optical and electronic properties, the issue of the size dependence of mechanical properties, including elasticity, is far less understood. It has been accepted that, in order for a mechanical property to approach the bulk value, a minimum number of molecules is required.[20,25−29] Using layer-by-layer stacking, a threshold number of 42 layers (17 nm) is required for NaCl materials to reach the bulk Young's modulus according to a modified continuum approach.[28]

In this paper, we report a systematic study of the size-dependent elastic compliance of organic thin film materials such as self-assembled monolayers (SAMs). The approach is unique in that we first produce materials of predesigned size, shape, and functionality using an atomic force microscopy (AFM) based nanofabrication technique referred to as nanografting.[30,31] The structure and dimensions of these preengineered nanostructures are then characterized using AFM, from which locations are selected for investigation of elasticity. Finally, the Young's modulus of these nanostructures in conjunction with the surrounding layer is extracted from the AFM measurements following the calculation described below. Because the nanostructures are well-defined, we hope this study provides more experimental evidence and insight into the subject of size-dependent mechanical properties.

Young's modulus, E, is a standard parameter used to quantify mechanical properties of various materials. Young's modulus represents elasticity and can be broadly defined as the ratio of stress over strain within the elastic limit of the material. This property can be experimentally measured as a function of the dimensions of the materials by varying the applied load.[32] For three-dimensional nanostructures, elasticity or Young's modulus may be viewed as the change in volumetric distortions within the elastic limit from the applied contact pressure. For materials in tension, Young's modulus can be expressed as

$$E = (L_0/\Delta L)/(F/A) \quad (1)$$

where L_0 is the equilibrium length, ΔL represents the length extension, F is the force applied, and A corresponds to the area of contact.

AFM is known for its high resolution in structural characterization as well as simultaneous imaging of mechanical properties.[33−36] In addition to topographic images, simultaneous friction[1,37−42] and elastic compliance[14,43−48] measurements of the surface can be taken. Quantifying local mechanical properties

† Part of the special issue "William Hase Festschrift".
‡ University of California.
§ National Institute of Standards and Technology.

10.1021/jp0544540 CCC: $33.50
Published on Web 11/16/2005

is less than straightforward due to the high contact pressure induced by the sharp tip, surface nonuniformity of the tip-contact area, and the lack of knowledge in the contact stiffness of the cantilever tip. Therefore, much research has been ongoing in instrument development, careful calibration, and models.[49−53]

In AFM measurements of Young's modulus, a modulation signal is introduced to the sample while the cantilever's response is monitored by recording the responsive amplitude and phase.[14,44] The spectrum of responsive amplitude versus driving frequency can also be acquired. To extract Young's modulus, two methods were reported: (a) calculating E from the amplitude and phase,[54] and (b) calculating E from the resonance frequencies for the tip−surface contact.[55,56] This paper uses the second method to deduce Young's modulus.

The first step is the determination of the force constant at the tip−surface contact point. By monitoring the cantilever response to the driving signal, frequency spectra are acquired, from which the resonance frequencies can be determined. Using a spring-mass model[53,55] to define the tip−surface contact, the force constant of the contact, k^*, can be related to the resonance frequency of the contact by:

$$k^* = ((f/f_c)^2 - 1)k_c \quad (2)$$

where k_c is the force constant of the cantilever, and f and f_c are the resonance frequencies of the cantilever and the contact, respectively. It is important to note that f is an experimentally determined parameter, and can be obtained from the resonance spectrum of the free cantilever when the tip is positioned sufficiently far from the surface. The f also depends on the medium surrounding the tip (e.g., air, water, or other solvent).[57]

The second step is the determination of the area of contact under the AFM tip. The AFM tip radius, R, must be determined in situ for each tip used from the topographic image of a surface step with known height.[58]

$$R = (h^2 + w^2)/(2h) \quad (3)$$

where h is the height of the step and w is the observed width of the step in AFM topography. The contact radius, a, under the AFM tip can then estimated using the Hertzian model

$$a = (3RL/4E^*)^{1/3} \quad (4)$$

where L is the imaging load obtained from force−distance curves and E^* is the reduced Young's modulus.

Finally, we may extract E^* treating the AFM tip−surface contact as an elastic sphere−plane with the Hertzian model[43,59]

$$E^* = k^*/(2a) \quad (5)$$

where E^* is the effective modulus of the tip−sample contact and a is the contact radius of the tip. Substituting eq 4 into eq 5 results in a solution for E^* based on experimentally measurable parameters:

$$E^* = (k^{*3}/6RL)^{1/2} \quad (6)$$

Experimental Section

Preparation of SAMs. Gold (Alfa Aesar, 99.999%) was deposited in a high-vacuum evaporator (Denton Vacuum Inc., Model DV502-A) at a base pressure of 2.6×10^{-5} Pa onto freshly cleaved mica substrates (clear ruby muscovite, Mica New York Corp.). The mica was preheated to 325 °C before deposition by using two quartz lamps to enhance the mobility of gold during the formation of terraced Au(111) domains.[31] A typical evaporation rate was 0.3 nm/s, and the thickness of the gold films ranged from 150 to 200 nm. After removal from the vacuum evaporator, the gold was immersed into freshly prepared thiol solutions.

The *n*-alkanethiols, *n*-decanethiol (abbreviated as $C_{10}SH$) and *n*-octadecanethiol ($C_{18}SH$), were purchased from Aldrich and used as received. Anhydrous ethanol, 2-butanol (99.6%), and hexadecane (99%) were purchased from Aldrich. Thiol solutions for SAM formation were prepared with concentrations ranging from 0.02 to 0.20 mM in solvents such as ethanol and 2-butanol. Gold substrates were immersed into these thiol solutions for a minimum of 48 h before imaging.

Atomic Force Microscopy. The atomic force microscope used in this study utilizes a home-built deflection-type scanning head with a commercial electronic controller (RHK Technology, Inc., Troy, MI).[60,61] Sharpened Si_3N_4 microcantilevers (MSCT) with a force constant of 0.1 N/m and a nominal resonance frequency of 38 kHz (Veeco, Santa Barbara, CA) were used in this study. A laser beam is focused onto the back of the cantilever and deflected to a four-segment photosensitive detector that can monitor the vertical deflection and lateral twisting of the cantilever as the tip scans across the surface.

Production and Characterization of Nanostructures with Designed Sizes. $C_{18}SH$ nanostructures with desired sizes and geometries were fabricated using the nanografting technique into matrix SAMs.[30,31] The SAMs used in this study were (1) a pure $C_{10}SH$ SAM, and (2) a mixed *n*-alkanethiol SAM consisting of $C_{10}SH$ and $C_{18}SH$. In nanografting, the surface covered with a SAM is first scanned with an AFM tip at low force to survey the topography of the surface. Once an appropriate fabrication area is identified, typically a single Au(111) terrace, the load is then increased to the threshold force. At this load, the tip will displace the thiol molecules from the gold surface via shearing during the scan. The threshold load was determined in each experiment by imaging a 5.0 nm × 5.0 nm area while systematically increasing the load.[62] For a well-structured SAM, the threshold load transition can be detected by observing the transition of the periodicity of the monolayer (0.5 nm) to that of the Au(111) lattice (0.3 nm). When this displacement is performed in a solution containing thiol molecules, the molecules in solution will self-assemble onto the newly exposed gold areas forming a nanostructure following the trajectory of the scan. The new structure is then scanned at low load to characterize the size and shape of the newly formed nanostructure. High-resolution images revealed that thiols in these nanostructures are also closely packed.[62]

Force Modulation Imaging. A detailed description of force modulation imaging (FMI) has been reported previously.[54,63] The sample is modulated with a sinusoidal signal of a fixed frequency in the Z-direction with the frequency, f, and amplitude, ΔZ, of modulation controlled by a lock-in amplifier. The modulation signal is normally set at frequencies above the response of the feedback circuit (several kilohertz) to minimize the coupling with the feedback circuit. The cantilever responds to the sinusoidal motion when the tip is in contact with the surface. During imaging, the amplitude and phase response of the cantilever are detected by the lock-in amplifier and then recorded as a function of the tip position. The response of the cantilever is sensitive to the local tip−surface contact. Three channels of data are acquired simultaneously, producing a topographic image and its corresponding amplitude and phase images.

Force Modulation Spectroscopy. Force modulation spectroscopy (FMS) can be acquired with the setup in Figure 1. Once the AFM tip is positioned on top of the structure of

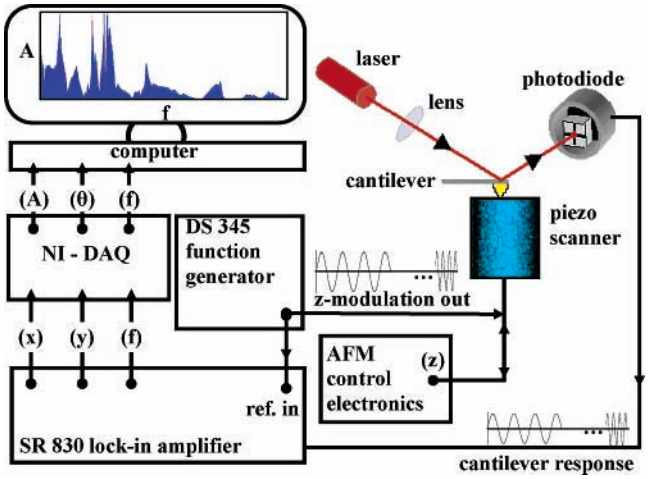

Figure 1. Schematic diagram of the AFM setup for force modulation spectroscopy (FMS). The instrument used consists of a home-built deflection-type AFM scanner controlled by RHK electronics and software. For FMS, a function generator (SRS DS345) is utilized to produce modulation signals. Cantilever response signal is amplified by a lock-in amplifier (SRS SR830) before entering the data acquisition card (NI-DAQ, National Instruments Measurement Studio). The amplitude and phase are plotted as a function of driving frequency, i.e., force modulation spectra.

interest, the computer controlled function generator initiates a frequency sweep. The function generator output is provided as a reference input to the lock-in amplifier and drives the piezo tube along the surface-normal direction. The tip responses at the tip−surface contact are detected by the photodiode and amplified by the lock-in amplifier. The signal from the cantilever response is recorded using a DAC board (National Instruments PCI-6024E Multiple I/O & DAQ interfaced with a CB-68LP I/O connector block), where the amplitude and phase are output to the computer and plotted as a function of sweeping frequency.

FMS provides a survey of the resonances present at the tip−surface contact. Using topographic images as guides, the AFM probe is parked at a designated point where FMS is acquired. The spectrum at a given point reveals the resonance frequencies of the local tip−surface contact in the imaging medium. The resonance frequencies extracted from the spectrum are utilized for accurate calculations of the tip−surface contact stiffness (see eq 2).

Most of the measurements are taken under low loads; thus the frictional component is negligible. For measurements taken at higher force, attempts were made to minimize the interaction of the normal and lateral signals. The control electronics employ a decoupling circuit to compensate for the coupling of normal and lateral signals from the cantilever. The cantilever deformation in both the normal and lateral directions was recorded during approach and retreat of the AFM tip. The lateral deformation was adjusted electronically while acquiring the deformation signal until the lateral signal diminished. All measurements for these experiments were done in solution to minimize the tip−sample adhesion.

Results and Discussion

To determine if there is a size dependence on the observed Young's modulus of nanostructures, a series of $C_{18}SH$ nanostructures with well-defined geometries have been fabricated into a $C_{10}SH$ matrix using the AFM-based lithographic technique of nanografting. A topographic image, Figure 2a, reveals nanostructures with the following dimensions: one 200 nm × 200 nm, one 100 nm × 100 nm, four adjacent 50 nm × 50 nm, and two adjacent 20 nm × 20 nm. These structures all display a height approximately 0.8 nm taller than the $C_{10}SH$ domains, which is consistent with the difference in chain length and the known 30° tilt of alkanethiolate SAMs on gold.[64] In addition to these well-defined structures fabricated into the matrix, additional structures with lateral dimensions ranging from 5 to 35 nm are formed in the matrix by exchange between the C_{10}-SH of the matrix and $C_{18}SH$ in solution.

After the nanostructures have been fabricated, the AFM tip is positioned on the center of these nanostructures denoted by the colored circles in Figure 2a. Successive zoom-in topographic images are acquired to ensure the accurate placement of the AFM tip. Once the tip is located on the desired point, FMS is acquired and the resonance responses of the tip−surface contact from 20.00 to 80.00 kHz are recorded. The spectra for each of the nanostructures denoted in Figure 2a are presented in Figure 2b.

Figure 2b reveals the similarity among those five selected nanostructures, i.e., overlaps in the observed peaks. Figure 2d reveals the spectra from 68.00 to 72.00 kHz, where resonances observed at the tip−surface contact overlap regardless of the nanostructures underneath. This observation indicates that the likely origin of these frequencies is the result of the mechanical resonances of the AFM assembly; therefore, they are not dependent on the nature of local contact. In contrast, a zoom-in view of the spectra from 23.00 to 27.00 kHz (Figure 2c) reveals the spectroscopic differences due to variation in nanostructure size. There are three resonances between 23.00 and 27.00 kHz, all of which exhibit the same trend in frequency shift due to the variation in the size of nanostructure. The C_{10}-SH matrix has a resonance at 24.36 kHz, followed by the 200 nm × 200 nm $C_{18}SH$ structure at 24.20 kHz. With the continuous decrease in the size of the nanostructures from 100 nm × 100 nm, to 50 nm × 50 nm and 20 nm × 20 nm, a red shift of resonance is observed, with 24.08, 24.00, and 23.96 kHz, respectively. This is an indication that smaller structures appear softer at the nanometer scale.

These resonance frequencies are utilized to calculate the Young's modulus of each nanostructure. To quantify the Young's modulus of the tip−surface contact for each of the nanostructures, the image load force, tip radius, frequency of the cantilever in solution, and frequency of the tip−surface contact must be determined. The resonance of the free cantilever, immersed in a hexadecanethiol solution in this experiment, was measured to be 18.00 kHz. Additionally, the imaging load, $L = 1.35$ nN, was obtained from force−displacement curves, and the tip radius, R, was calculated to be 62.94 nm. Following eqs 2 and 6, the tip−surface contact stiffness and the Young's modulus of the tip−surface contact were calculated. The results of these calculations, along with the dimensions of the nanostructures probed, are shown in Table 1. The number of $C_{18}SH$ molecules in each structure, assuming a close-packed geometry with lattice spacing of 0.499 nm, is also included.

TABLE 1: Calculated Contact Stiffness and Young's Modulus for Engineered Nanostructures

nanostructure (nm × nm)	area (nm^2)	no. of molecules	mass (10^{-18} g)	F (kHz)	k^* (N/m)	E^* (GPa)	% edge	% bulk
$C_{10}SH$ matrix				24.36	0.0831	1.07		
200 × 200	4.00×10^4	1.60×10^5	76.4	24.20	0.0807	1.02	79.8	20.3
100 × 100	1.00×10^4	4.00×10^4	19.1	24.08	0.0789	0.99	39.2	60.8
50 × 50	2.50×10^3	1.00×10^4	4.78	24.00	0.0778	0.96	20.8	79.2
20 × 20	4.00×10^2	1.60×10^3	0.764	23.96	0.0772	0.95	10.7	89.3

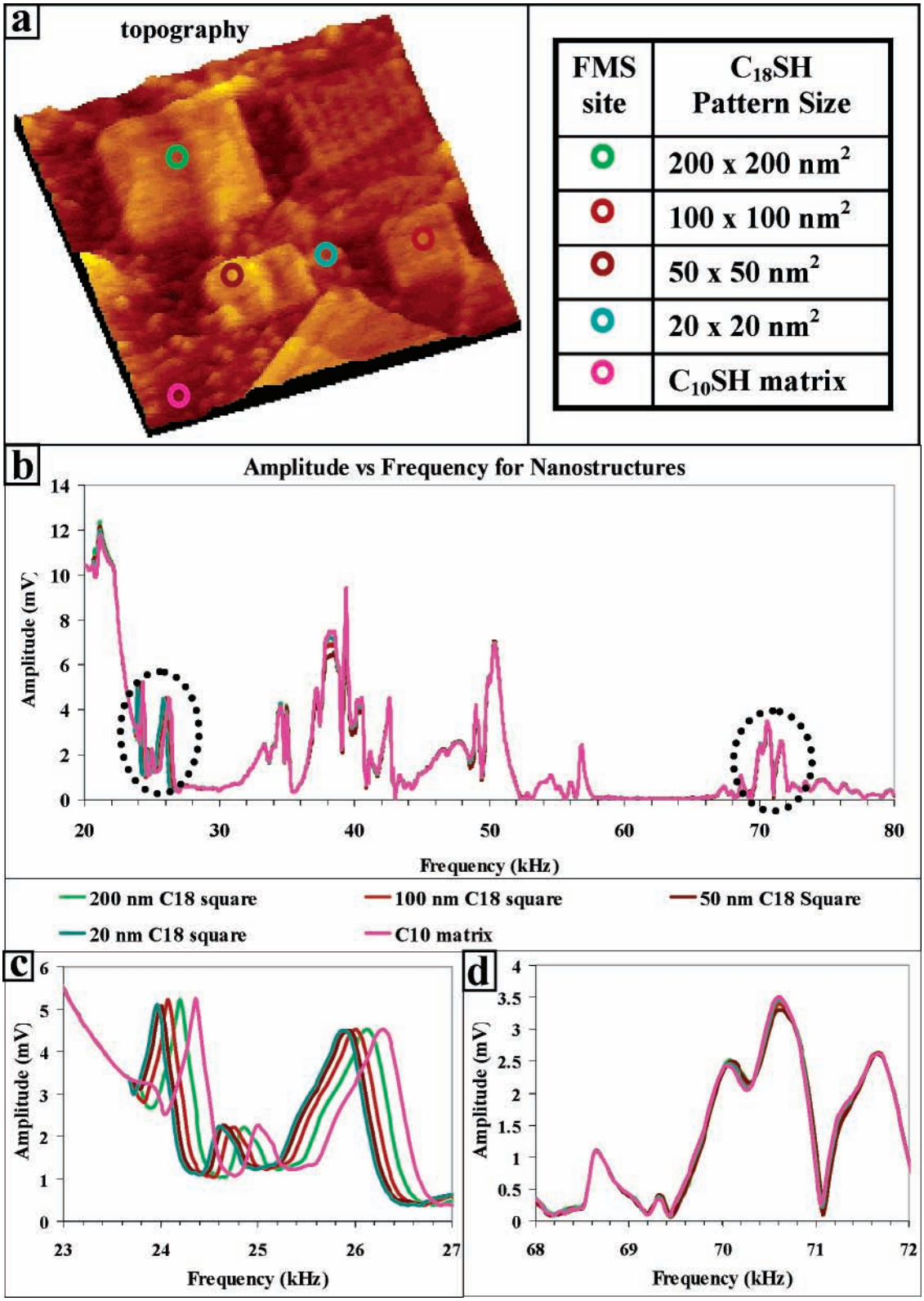

Figure 2. FMS measurements acquired from nanostructures with designed sizes and geometries. (a) Topographic image of $C_{18}SH$ nanostructures fabricated into a $C_{10}SH$ matrix. Image was acquired at a load of 1.35 nN with a 600 × 600 nm^2 total scan area. (b) FMS from 20 to 80 kHz on selected nanostructures indicated in (a) following the same color code. (c) Zoom-in of FMS from 23 to 27 kHz, where the spectra show a size dependence. (d) Zoom-in of FMS from 68 to 72 kHz, where measured spectra do not vary with nanostructures.

The Young's modulus has been plotted as a function of nanostructure size and mass, and is presented in Figure 3. The plots clearly reveal that Young's modulus decreases nonlinearly with size (see Figure 3a), and with mass (see Figure 3b) of the nanostructure. Mathematical fitting reveals an $E^* = 0.014 \ln(x) + 0.859$ relationship. Increasing the size of $C_{18}SH$ nanostructure beyond the critical value should result in a Young's modulus equivalent to that of a two-dimensional (2D) bulk of SAM. In fact, the E^* value did approach the bulk value with a 300 nm × 300 nm or larger nanostructure.

We have evaluated if the observed size dependence is due to the ratio change in 2D domain boundaries, similar to the line

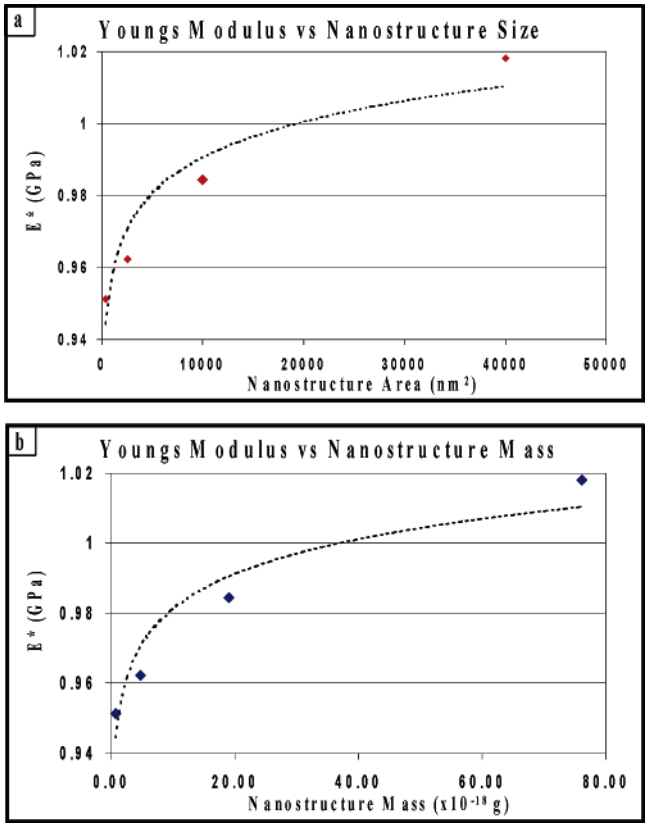

Figure 3. Young's modulus as a function of size of the nanostructures. Young's modulus of the structures measured from the experiment shown in Figure 2a are plotted against the area of the nanostructure in (a) and the mass of the nanostructure in (b). This trend is reproducible in all experiments. Dotted lines showing the general logarithmic dependence of the data have also been included in the graphs. For (a) $E^* = 0.014 \ln(x) + 0.859$; for (b) $E^* = 0.014 \ln(x) + 0.948$.

tension issue present in membrane rafts.[65,66] Force modulation experiments on nanostructures have shown that the edges of nanostructures appear softer than the bulk areas. In the case of $C_{18}SH$ nanostructures fabricated into a C_6SH matrix, FMI was able to quantify the width of the boundary to be 5.5 nm because the resonance occurred at a lower frequency than the bulk areas.[63] The dimensions of these boundaries are similar to those that have been calculated using a line tension approximation for rafts in lipid bilayers.[65,66] In the case where the lipid molecules in the raft are 1 nm taller than the surrounding matrix, a boundary of 2−4 nm is expected.[65,66] While the boundary percentage does increase with decreasing nanostructure size, the 2D bulk areas also decrease following similar mathematics of the E^*. Given also the fact that the tip is parked at the center of the nanostructure, we conclude that the observed size dependence is genuine, and reflects the 2D bulk property.

Although quantized fracture models and modified continuum models were elegantly demonstrated for hard materials,[25,28] to the best of our knowledge there are few models developed for soft materials that can predict elasticity in the nanoregime. One way to rationalize our observations is to consider each nanostructure as an independent entity inside the matrix, because of the van der Waals interactions among the chains. Although the $C_{18}SH$ molecules are embedded into a $C_{10}SH$ matrix, the extra interchain interactions among the top eight carbon atoms in the $C_{18}SH$ molecules are sufficient to consider these nanostructure as separate composite from the matrix SAM. Following the logic presented by Sun et al.,[28] each molecule in the pattern will interact under pressure with its neighbors. At nanometer-length scales there are no longer sufficient neighbors to react to the applied pressure with the same behavior as a bulk film would have. This results in a decrease of the observed Young's modulus of the structure. The trends observed in these computational studies show that, as the dimensions of materials decrease to the nanoscale, the Young's modulus of these materials also decreases.[23,67] The experimental results in this work also display this trend quantitatively. Hopefully, the results of this work will trigger theoretical simulations of the finite size effects observed in soft and composite materials.

To demonstrate the robustness of the size-dependent effect, FMI was acquired at various frequencies. Figure 4 shows the FMI of a series of $C_{18}SH$ nanostructures, with sizes of 70 nm × 50 nm, 90 nm × 75 nm, 95 nm × 105 nm, 120 nm × 100 nm, and 175 nm × 225 nm, fabricated into a mixed 9:1 $C_{10}SH$:$C_{18}SH$ matrix. In the top row, at a modulation frequency of 26.60 kHz, the 95 nm × 105 nm structure is on resonance and displays the brightest contrast in the amplitude image. At 27.5 kHz the 120 nm × 100 nm structure is on resonance. The larger nanostructures display resonance responses at higher frequencies, and the smaller nanostructures display resonance responses at lower frequencies. The fact that a smaller nanostructure was turned on at a lower frequency than a larger one is consistent with the FMS studies described above. As a bonus based on this observation, one can actively tune the amplitude contrast in FMI by varying the size.[63] Our measurements of Young's modulus are very close to those in previous reports; e.g., a contact bulk elasticity of 1.32 GPa was reported for a Si_3N_4 tip in contact with *n*-decanethiol SAM.[10,68,69] Considering the differences in approach and the validity of the Hertzian model, the agreement is better than expected, which also suggests the validity of the continuum mechanics model.

This observation of the size dependence of the Young's modulus of the nanostructures is very significant. It indicates that we can no longer assume elasticity is constant at the nanometer scale. Therefore, one should take size-dependent elastic compliance into consideration for the design of nanodevices, MEMS, and NEMS. Similar approaches may be used to investigate if an analogous relationship is present in other properties, such as shear modulus, G^*. We anticipate a positive answer to this inquiry.

Conclusions

Using AFM imaging and nanolithography, we have investigated the issue of size-dependent elasticity at the nanometer scale. Our approach is to first fabricate nanostructures of $C_{18}SH$ with designed sizes and shapes into *n*-alkanethiol SAMs. These preengineered materials are then imaged by AFM for high-resolution structure characterization and for the selection of the tip location in measuring the local mechanical property. FMI reveals that the resonance frequency of the tip−surface contact varies with the size of the nanostructure. Smaller nanostructures appear softer than larger ones as the resonance occurs at lower frequencies. Using FMS, the spectra of the tip−surface contacts were also acquired for these preengineered the nanostructures, from which Young's modulus can be calculated using continuum mechanics models. The Young's modulus is found to decrease nonlinearly as the size of nanostructures decreases. This observation indicates that materials appear softer than bulk when the grain size decreases to nanometer scale. This approach is unique in that the nanostructures are precisely engineered for systematic investigations. The results represent conclusive evidence of the size dependence of elasticity. Work is in progress to investigate the effect of chain length, positive versus negative nanostructures, and various functionalities. The

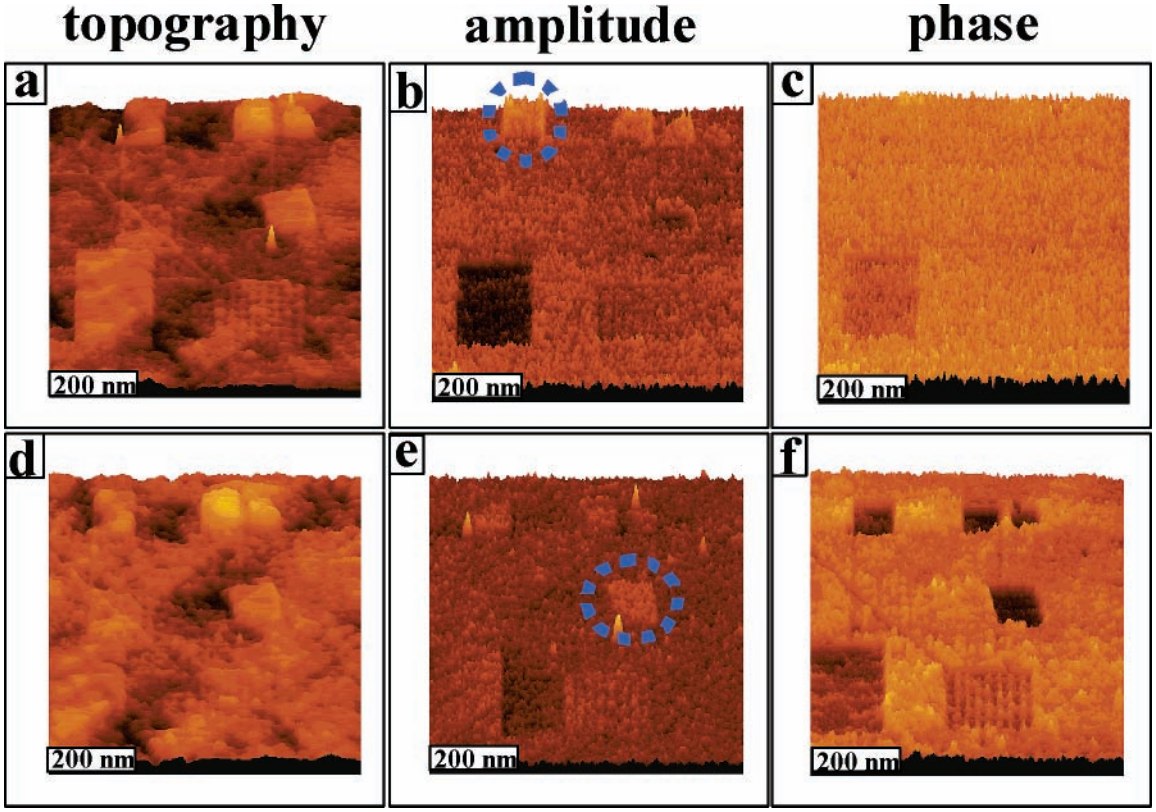

Figure 4. FMI of $C_{18}SH$ nanostructures fabricated into a 9:1 $C_{10}SH$:$C_{18}SH$ mixed thiol SAM. Image area is 700 × 700 nm^2, and modulation frequencies are 26.60 kHz (a−c) and 27.50 kHz (d−f). Nanostructures range from 70 nm × 50 nm to 175 nm × 225 nm. Blue dotted circles in amplitude images highlight the nanostructures that exhibit resonance at the imaging modulation frequency.

approach utilized may be applied to study the size dependence of various materials and other mechanical properties.

Acknowledgment. The authors greatly appreciate the technical assistance of and stimulating discussions with Jing-jiang Yu and Amanda Price at UC Davis. This work was supported by the University of California, Davis, and the Nanotechnology Initiative of the National Institute of Standards and Technology, Materials Science and Engineering Laboratory, in conjunction with the NIST nanotribology research program. Additional support was provided by National Science Foundation through NER-DMI-0304345, CHE-0244830, and CHE-0210807, and a seed fund from CPIMA via Stanford University (NSF-MRSEC DMR-0213618). W.J.P. acknowledges support from the Tyco Electronics Graduate Fellowship in Functional Materials. (Statement per the request of the NIST grant. Certain commercial equipment, instruments, or materials are identified in this paper in order to specify the experimental procedure adequately. Such identification is not intended to imply recommendation or endorsement by the National Institute of Standards and Technology, nor is it intended to imply that the materials or equipment identified are necessarily the best available for the purpose.)

References and Notes

(1) Tambe, N. S.; Bhushan, B. *Appl. Phys. Lett.* **2005**, *86*, 1931021.
(2) Gruen, D. M. *Annu. Rev. Mater. Sci.* **1999**, *29*, 211.
(3) Krauss, A. R.; Auciello, O.; Guruen, D. M.; Jayatissa, A.; Sumant, A.; Tucek, J.; Mancini, D. C.; Moldovan, N.; Erdermir, A.; Ersoy, D.; Gardos, M. N.; Busmann, H. G.; Meyer, E. M.; Ding, M. Q. *Diamond Relat. Mater.* **2001**, *10*, 1952.
(4) Terrones, M. *Annu. Rev. Mater. Res.* **2003**, *33*, 419.
(5) Wang, Z. L.; Poncharal, P.; de Heer, W. A. *J. Phys. Chem. Solids* **2000**, *61*, 1025.
(6) Miller, S. A.; Ding, J. H.; Gin, D. L. *Curr. Opin. Colloid Interface Sci.* **1999**, *4*, 338.
(7) Gimzewski, J. K.; Joachim, C. *Science* **1999**, *283*, 1683.
(8) Unertl, W. N. *J. Vac. Sci. Technol., A* **1999**, *17*, 1779.
(9) Shenoy, V. B.; Miller, R.; Tadmor, E. B.; Phillips, R.; Ortiz, M. *Phys. Rev. Lett.* **1998**, *80*, 742.
(10) Ogletree, D. F.; Carpick, R. W.; Salmeron, M. *Rev. Sci. Instrum.* **1996**, *67*, 3298.
(11) Luan, B. Q.; Robbins, M. O. *Nature* **2005**, *435*, 929.
(12) Wu, H. A.; Liu, G. R.; Wang, J. S. *Modell. Simul. Mater. Sci. Eng.* **2004**, *12*, 225.
(13) Banin, U.; Lee, C. J.; Guzelian, A. A.; Kadavanich, A. V.; Alivisatos, A. P.; Jaskolski, W.; Bryant, G. W.; Efros, A. L.; Rosen, M. *J. Chem. Phys.* **1998**, *109*, 2306.
(14) DeVecchio, D.; Bhushan, B. *Rev. Sci. Instrum.* **1997**, *68*, 4498.
(15) Alivisatos, A. P. *Science* **1996**, *271*, 933.
(16) Hendriksen, P. V.; Linderoth, S.; Lindgard, P. A. *Phys. Rev. B* **1993**, *48*, 7259.
(17) Brus, L. E.; Szajowski, P. F.; Wilson, W. L.; Harris, T. D.; Schuppler, S.; Citrin, P. H. *J. Am. Chem. Soc.* **1995**, *117*, 2915.
(18) Moriarty, P. *Rep. Prog. Phys.* **2001**, *64*, 297.
(19) Nirmal, M.; Murray, C. B.; Bawendi, M. G. *Phys. Rev. B* **1994**, *50*, 2293.
(20) Piner, R. D.; Xu, T. T.; Fisher, F. T.; Qiao, Y.; Ruoff, R. S. *Langmuir* **2003**, *19*, 7995.
(21) Schaaff, T. G.; Shafigullin, M. N.; Khoury, J. T.; Vezmar, I.; Whetten, R. L.; Cullen, W. G.; First, P. N.; Gutierrez-Wing, C.; Ascensio, J.; Jose-Yacaman, M. J. *J. Phys. Chem. B* **1997**, *101*, 7885.
(22) Wang, Y.; Herron, N. *J. Phys. Chem.* **1991**, *95*, 525.
(23) Bohme, T. R.; de Pablo, J. J. *J. Chem. Phys.* **2002**, *116*, 9939.
(24) Antes, I.; Thiel, W. *J. Phys. Chem. A* **1999**, *103*, 9290.
(25) Pugno, N. M.; Ruoff, R. S. *Philos. Mag.* **2004**, *84*, 2829.
(26) Lu, W.; Komvopoulos, K. *J. Appl. Phys.* **1999**, *86*, 2268.
(27) Yan, W.; Komvopoulos, K. *J. Tribol.: Trans. ASME* **1998**, *120*, 385.
(28) Sun, C. T.; Zhang, H. *J. Appl. Phys.* **2003**, *93*, 1212.
(29) Lu, W.; Komvopoulos, K.; Patsalas, P.; Charitidis, C.; Gioti, M.; Logothetidis, S. *Surf. Coat. Technol.* **2003**, *168*, 12.
(30) Xu, S.; Laibinis, P. E.; Liu, G. Y. *J. Am. Chem. Soc.* **1998**, *120*, 9356.
(31) Xu, S.; Liu, G. Y. *Langmuir* **1997**, *13*, 127.
(32) Israelachvili, J. N. *Surf. Sci. Rep.* **1992**, *14*, 109.

(33) Salvetat, J. P.; Bonard, J. M.; Thomson, N. H.; Kulik, A. J.; Forro, L.; Benoit, W.; Zuppiroli, L. *Appl. Phys. A: Mater. Sci. Process.* **1999**, *69*, 255.
(34) Magonov, S. N.; Reneker, D. H. *Annu. Rev. Mater. Sci.* **1997**, *27*, 175.
(35) Bhushan, B.; Koinkar, V. N. *Appl. Phys. Lett.* **1994**, *64*, 1653.
(36) Weisenhorn, A. L.; Egger, M.; Ohnesorge, F.; Gould, S. A. C.; Heyn, S. P.; Hansma, H. G.; Sinsheimer, R. L.; Gaub, H. E.; Hansma, P. K. *Langmuir* **1991**, *7*, 8.
(37) Carpick, R. W.; Salmeron, M. *Chem. Rev.* **1997**, *97*, 1163.
(38) Frommer, J. *Angew. Chem., Int. Ed. Engl.* **1992**, *31*, 1298.
(39) Quate, C. F. *Surf. Sci.* **1994**, *300*, 980.
(40) Ruan, J. A.; Bhushan, B. *J. Tribol.: Trans. ASME* **1994**, *116*, 378.
(41) Meyer, G.; Amer, N. M. *Appl. Phys. Lett.* **1988**, *53*, 1045.
(42) Bhushan, B.; Israelachvili, J. N.; Landman, U. *Nature* **1995**, *374*, 607.
(43) Carpick, R. W.; Ogletree, D. F.; Salmeron, M. *Appl. Phys. Lett.* **1997**, *70*, 1548.
(44) Bar, G.; Rubin, S.; Parikh, A. N.; Swanson, B. I.; Zawodzinski, T. A.; Whangbo, M. H. *Langmuir* **1997**, *13*, 373.
(45) Overney, R. M.; Meyer, E.; Frommer, J.; Guntherodt, H. J.; Fujihira, M.; Takano, H.; Gotoh, Y. *Langmuir* **1994**, *10*, 1281.
(46) Gould, S. A. C.; Drake, B.; Prater, C. B.; Weisenhorn, A. L.; Manne, S.; Kelderman, G. L.; Butt, H. J.; Hansma, H.; Hansma, P. K.; Magonov, S.; Cantow, H. J. *Ultramicroscopy* **1990**, *33*, 93.
(47) Radmacher, M.; Tillmann, R. W.; Fritz, M.; Gaub, H. E. *Science* **1992**, *257*, 1900.
(48) Radmacher, M.; Tilmann, R. W.; Gaub, H. E. *Biophys. J.* **1993**, *64*, 735.
(49) Asif, S. A.; Wahl, K. J.; Colton, R. J.; Warren, O. L. *J. App. Phys.* **2001**, *90*, 1192.
(50) Asif, S. A. S.; Wahl, K. J.; Colton, R. J. *Rev. Sci. Instrum.* **1999**, *70*, 2408.
(51) Asif, S. A. S.; Wahl, K. J.; Colton, R. J.; Warren, O. L. *J. Appl. Phys.* **2001**, *90*, 1192.
(52) Marcus, M. S.; Carpick, R. W.; Sasaki, D. Y.; Eriksson, M. A. *Phys. Rev. Lett.* **2002**, *88*, 226103.
(53) Muraoka, M. *Nanotechnology* **2005**, *16*, 542.
(54) Jourdan, J. S.; Cruchon-Dupeyrat, S. J.; Huan, Y.; Kuo, P. K.; Liu, G. Y. *Langmuir* **1999**, *15*, 6495.
(55) Muraoka, M.; Arnold, W. *JSME Int. J., Ser. A* **2001**, *44*, 396.
(56) Rabe, U.; Kopycinska, M.; Hirsekorn, S.; Arnold, W. *Ultrasonics* **2002**, *40*, 49.
(57) Tamayo, J.; Humphris, A. D. L.; Miles, M. J. *Appl. Phys. Lett.* **2000**, *77*, 582.
(58) Xu, S.; Amro, N. A.; Liu, G. Y. *Appl. Surf. Sci.* **2001**, *175*, 649.
(59) Hu, J.; Xiao, X. D.; Salmeron, M. *Appl. Phys. Lett.* **1995**, *67*, 476.
(60) Xu, S.; Cruchon-Dupeyrat, S. J. N.; Garno, J. C.; Liu, G. Y.; Jennings, G. K.; Yong, T. H.; Laibinis, P. E. *J. Chem. Phys.* **1998**, *108*, 5002.
(61) Salmeron, M.; Folch, A.; Neubauer, G.; Tomitori, M.; Ogletree, D. F.; Kolbe, W. *Langmuir* **1992**, *8*, 2832.
(62) Xu, S.; Miller, S.; Laibinis, P. E.; Liu, G. Y. *Langmuir* **1999**, *15*, 7244.
(63) Price, W. J.; Kuo, P. K.; Lee, T. R.; Colorado, R.; Ying, Z. C.; Liu, G. Y. *Langmuir* **2005**, *21*, 8422.
(64) Poirier, G. E.; Tarlov, M. J. *Langmuir* **1994**, *10*, 2853.
(65) Akimov, S. A.; Kuzmin, P. I.; Zimmerberg, J.; Cohen, F. S.; Chizmadzhev, Y. A. *J. Electroanal. Chem.* **2004**, *564*, 13.
(66) Kuzmin, P. I.; Akimov, S. A.; Chizmadzhev, Y. A.; Zimmerberg, J.; Cohen, F. S. *Biophys. J.* **2005**, *88*, 1120.
(67) Van Workum, K.; de Pablo, J. J. *Nano Lett.* **2003**, *3*, 1405.
(68) Carpick, R. W.; Agrait, N.; Ogletree, D. F.; Salmeron, M. *Langmuir* **1996**, *12*, 3334.
(69) Kiridena, W.; Jain, V.; Kuo, P. K.; Liu, G. Y. *Surf. Interface Anal.* **1997**, *25*, 383.